Development of equilibrium after preheating

Gary Felder

Department of Physics, Stanford University, Stanford, California 94305
and CITA, University of Toronto, 60 Saint George Street, Toronto, Ontario, Canada M5S 3H8

Lev Kofman

CITA, University of Toronto, 60 Saint George Street, Toronto, Ontario, Canada M5S 3H8
(Received 29 November 2000; published 12 April 2001)

We present a fully nonlinear study of the development of equilibrium after preheating. Preheating is the exponentially rapid transfer of energy from the nearly homogeneous inflaton field to fluctuations of other fields and/or the inflaton itself. This rapid transfer leaves these fields in a highly nonthermal state with energy concentrated in infrared modes. We have performed lattice simulations of the evolution of interacting scalar fields during and after preheating for a variety of inflationary models. We have formulated a set of generic rules that govern the thermalization process in all of these models. Notably, we see that once one of the fields is amplified through parametric resonance or other mechanisms, it rapidly excites other coupled fields to exponentially large occupation numbers. These fields quickly acquire nearly thermal spectra in the infrared, which gradually propagates into higher momenta. Prior to the formation of total equilibrium, the excited fields group into subsets with almost identical characteristics (e.g. group effective temperature). The way fields form into these groups and the properties of the groups depend on the couplings between them. We also studied the onset of chaos after preheating by calculating the Lyapunov exponent of the scalar fields.

I. INTRODUCTION

The theory of inflation has been highly successful in explaining many of the initial conditions for the hot big bang model as well as providing a mechanism by which the seeds of large scale structure were formed. Typical models of inflation are based on the slow-roll evolution of the homogeneous inflaton scalar field(s) ϕ. Inflation ends when the slow-roll regime is dynamically terminated and the field(s) begins to oscillate around the minimum of its effective potential $V(\phi)$ as in chaotic inflation [1] or ''waterfalls'' towards the minimum of V as in hybrid inflation [2]. After inflation the homogeneous inflaton field(s) decays due to its interactions with other fields or its self-interaction. If the inflaton decay into other fields were slow as in perturbation theory, the created particles would settle into thermal equilibrium as the inflaton decayed. However, the decay of the inflaton typically occurs via rapid, non-perturbative mechanisms collectively known as preheating [3]. The character of preheating may vary from model to model, e.g. parametric excitation in chaotic inflation [4] and another, specific type of preheating in hybrid inflation [5], but its distinct feature remains the same: rapid amplification of one or more bosonic fields to exponentially large occupation numbers. This amplification is eventually shut down by back reaction of the produced fluctuations. The end result of the process is a turbulent medium of coupled, inhomogeneous, classical waves far from equilibrium [6].

Despite the development of our understanding of preheating after inflation, the transition from this stage to a hot Friedmann universe in thermal equilibrium has remained relatively poorly understood. A theory of the thermalization of the fields generated from preheating is necessary to bridge the gap between inflation and the hot big bang. The details of

this thermalization stage depend on the constituents of the fundamental Lagrangian $\mathcal{L}(\phi_i, \chi_i, \psi_i, A_\mu, h_{\mu\nu}, \dots)$ and their couplings, so at first glance it would seem that a description of this process would have to be strongly model dependent. We have found, however, that many features of this stage seem to hold generically across a wide spectrum of models. This fact is understandable because the conditions at the end of preheating are generally not qualitatively sensitive to the details of inflation. Indeed, at the end of preheating and beginning of the turbulent stage (denoted by t_*), the fields are out of equilibrium. We have examined many models and found that at t_* there is not much trace of the linear stage of preheating and conditions at t_* are not qualitatively sensitive to the details of inflation. We therefore expect that this second, highly nonlinear, turbulent stage of preheating may exhibit some universal, model-independent features.

Although a realistic model would include one or more Higgs-Yang-Mills sectors, we treat the simpler case of interacting scalars. Within this context, however, we consider a number of different models including several chaotic and hybrid inflation scenarios with a variety of couplings between the inflaton and other matter fields.

There are many questions about the thermalization process that we set out to answer in our work. Could the turbulent waves that arise after preheating be described by the theory of (transient) Kolmogorov turbulence or would they directly approach thermal equilibrium? Could the relaxation time towards equilibrium be described by the naive estimate $\tau \sim (n\sigma_{int})^{-1}$, where n is a density of scalar particles and σ_{int} is a cross section of their interaction? If the inflaton ϕ were decaying into a field χ, what effect would the presence of a decay channel σ for the χ field have on the thermalization process? For that matter, would the presence of σ significantly alter the preheating of χ itself or even destroy it as

63 103503-1

suggested in [7]? How strongly model dependent is the process of thermalization; are there any universal features across different models? Finally there is the question of chaos. It is known that Higgs-Yang-Mills systems display chaotic dynamics during thermalization [8]. The possibility of chaos in the case of a single, self-interacting inflaton was mentioned in passing in [6], but when we began our work it was unclear at what stage of preheating chaos might appear, and in what way.

Because the systems we are studying involve strong, nonlinear interactions far from thermal equilibrium, it is not possible to solve the equations of motion using linear analysis in Fourier space. Instead we solve the scalar field equations of motion directly in position space using lattice simulations. These simulations automatically take into account all nonlinear effects of scattering and back reaction. Using these numerical results we have been able to formulate a set of empirical rules that seem to govern thermalization after inflation. These rules qualitatively describe thermalization in a wide variety of models. The features of this process are in some cases very different from our initial expectations.

Section II gives a brief review of preheating in different inflationary models. This review should serve to motivate our study and place it in the broader context of inflationary cosmology. Sections III and IV describe the results of our numerical calculations. Section III describes one simple chaotic inflation model that we chose to focus on as a clear illustration of our results, while Sec. IV discusses how the thermalization process occurs in a variety of other models. Section V describes the onset of chaos during preheating and includes a discussion of the measurement and interpretation of the Lyapunov exponent in this context. Section VI contains a list of empirical rules that we have formulated to describe thermalization after preheating. Section VII discusses these results and other aspects of non-equilibrium scalar field dynamics. Finally, there is an appendix that describes our lattice simulations.

II. INFLATION AND PREHEATING

In this section we outline the context where the problem of thermalization after inflation arises. In the inflationary scenario, the very early universe expands (quasi)exponentially due to a vacuum-like equation of state. Such an equation of state can arise in a number of different ways, most of which are based on a homogeneous condensate of one or more classical scalar fields. We will consider two types of inflationary models. The first is chaotic inflation [1] with the single scalar field potential $V(\phi)$. The second is hybrid inflation, which involves several scalar fields [2]. The properties of these models are widely discussed in the literature. We will be dealing only with the decay of the homogeneous inflaton condensate into inhomogeneous modes of the same or other scalars and the subsequent interactions of these inhomogeneous modes as they approach thermal equilibrium. Any particles present before or during inflation are diluted by the exponential expansion. Thus by the end of inflation all energy is contained in the potential $V(\phi, \ldots)$ of one or more classical, slowly moving, homogeneous inflaton fields. Immediately after inflation the background field(s) is moving fast and produces particles of the fields coupled to it. These created particles are mutually interacting and ultimately must end up in thermal equilibrium. However, particles may be created so fast that they spend some time in non-equilibrium states with very large occupation numbers.

Consider chaotic inflation with the potential

$$V(\phi) = \frac{m^2}{2} \phi^2 + \frac{\lambda}{4} \phi^4. \tag{1}$$

Soon after the end of inflation the homogeneous inflaton field $\phi(t)$ coherently oscillates around the minimum of its potential with an amplitude on the order of a Planck mass. The inflaton oscillations decay due to the creation of particles interacting with ϕ. Let χ be another scalar field coupling with the inflaton field as $\frac{1}{2} g^2 \phi^2 \chi^2$. Particles of the χ field are produced from the interaction of the quantum vacuum state of χ with the coherently oscillating classical field ϕ. The dominant channel for this production is the non-perturbative mechanism of parametric excitation. The χ_k mode functions exponentially increase with time as $\chi_k \simeq e^{\mu_k t}$, where the characteristic exponent μ_k is a model-dependent function [4,9]. The copious production of χ particles constitutes the first stage of preheating after inflation [3]. This state can be studied with analytical methods developed in [4,9,10]. However, very soon the amplitudes of the inhomogeneous modes (i.e., the occupation number n_k) of χ become so large that the back reaction of created particles must be taken into account. The most important back-reaction effect will be the rescattering of particles $\chi\phi \rightarrow \chi\phi$ [6], which is difficult to describe analytically [4]. Thus, to follow the evolution of the interacting scalar fields after the first stage of preheating (dominated by parametric resonance), one must investigate the full non-linear dynamics of the interacting scalars.

The Hartree approximation, which is often used for problems of nonequilibrium quantum field theory, is insufficient here for several reasons. It fails when field fluctuations have amplitudes comparable with that of the background field, which occurs exponentially fast in our case. It does not take into account the rescattering of particles. Moreover, in the context of preheating there are diagrams beyond the Hartree approximation that survive in the $N \rightarrow \infty$ limit and give comparable contributions to those included in the Hartree approximation [4,9].

Fortunately, scalar fields with high occupation numbers can be interpreted as classical waves, and the problem can be treated with lattice simulations [11]. Such simulations provide approximate solutions to nonequilibrium quantum field theory problems, and we believe they include the leading physical effects.

Hybrid inflation models involve multiple scalar fields. The simplest potential for two-field hybrid inflation is

$$V(\phi, \sigma) = \frac{\lambda}{4} (\sigma^2 - v^2)^2 + \frac{g^2}{2} \phi^2 \sigma^2. \tag{2}$$

Inflation in this model occurs while the homogeneous ϕ field slow rolls from large ϕ towards the bifurcation point at ϕ

$=(\sqrt{\lambda}/g)v$ (due to the slight lift of the potential in ϕ direction). Once $\phi(t)$ crosses the bifurcation point, the curvature of the σ field, $m_\sigma^2 \equiv \partial^2 V/\partial\sigma^2$, becomes negative. This negative curvature results in exponential growth of σ fluctuations. Inflation then ends abruptly in a ''waterfall'' manner. It was recently found [5] that there is strong preheating in hybrid inflation, but its character is quite different from preheating based on parametric resonance.

One reason to be interested in hybrid inflation is that it can be easily implemented in supersymmetric theories. In particular, for illustration we will use supersymmetric F-term inflation as an example of a hybrid model.

III. CALCULATIONS IN CHAOTIC INFLATION

In this section we present the results of our numerical lattice simulations of the dynamics of interacting scalars after inflation. We discuss in detail one simple model that we have chosen to illustrate the general properties of thermalization after preheating. The next section will discuss thermalization in the context of other models.

A. Model

The example we have chosen to focus on is chaotic inflation with a quartic inflaton potential. The inflaton ϕ has a four-leg coupling to another scalar field χ, which in turn can couple to one or more other scalars σ_i. The potential for this model is

$$V = \frac{1}{4}\lambda\phi^4 + \frac{1}{2}g^2\phi^2\chi^2 + \frac{1}{2}h_i^2\chi^2\sigma_i^2. \tag{3}$$

The equations of motion for the model (3) are given by

$$\ddot{\phi} + 3\frac{\dot{a}}{a}\dot{\phi} - \frac{1}{a^2}\nabla^2\phi + (\lambda\phi^2 + g^2\chi^2)\phi = 0 \tag{4}$$

$$\ddot{\chi} + 3\frac{\dot{a}}{a}\dot{\chi} - \frac{1}{a^2}\nabla^2\chi + (g^2\phi^2 + h_i^2\sigma_i^2)\chi = 0 \tag{5}$$

$$\ddot{\sigma_i} + 3\frac{\dot{a}}{a}\dot{\sigma_i} - \frac{1}{a^2}\nabla^2\sigma_i + (h_i^2\chi^2)\sigma_i = 0. \tag{6}$$

We also included self-consistently the evolution of the scale factor $a(t)$. The model described by these equations is a conformal theory, meaning that the expansion of the universe can be (almost) eliminated from the equations of motion by an appropriate choice of variables [9]. See the Appendix for more information on the lattice simulations we used to solve these equations, including information on the initial conditions and the rescaled units we used in the calculations and in the plots we show here.

Preheating in this theory in the absence of the σ_i fields was described in [9]. For $g^2 \gtrsim \lambda$ the field χ will experience parametric amplification, rapidly rising to exponentially large occupation numbers. In the absence of the χ field (or for sufficiently small g) ϕ will be resonantly amplified through its own self-interaction, but this self-amplification is

much less efficient than the two-field interaction. The results shown here are for $\lambda = 9 \times 10^{-14}$ [for Cosmic Background Explorer (COBE) normalization] and $g^2 = 200\lambda$. When we add a third field we use $h_1^2 = 100g^2$ and when we add a fourth field we use $h_2^2 = 200g^2$.

B. Output variables

There are a number of ways to illustrate the behavior of scalar fields, and different ones are useful for exploring different phenomena. The raw data are the value of the field $f(t,\vec{x})$ or, equivalently, its Fourier transform $f_k(t)$. One of the simplest quantities one can extract from these values is the variance

$$\langle[f(t) - \bar{f}(t)]^2\rangle = \frac{1}{(2\pi)^3}\int d^3k |f_k(t)|^2, \tag{7}$$

where the integral does not include the contribution of a possible delta function at $\vec{k} = 0$, representing the mean value $\bar{f}$.

One of the most interesting variables to calculate is the (comoving) number density of particles of the f field,

$$n_f(t) \equiv \frac{1}{(2\pi)^3}\int d^3k\, n_k(t), \tag{8}$$

where n_k is the (comoving) occupation number of particles:

$$n_k(t) \equiv \frac{1}{2\omega_k}|\dot{f}_k|^2 + \frac{\omega_k}{2}|f_k|^2 \tag{9}$$

$$\omega_k \equiv \sqrt{k^2 + m_{eff}^2} \tag{10}$$

$$m_{eff}^2 \equiv \frac{\partial^2 V}{\partial f^2}. \tag{11}$$

For the model (3) this effective mass is given by

$$m_{eff}^2 = \begin{cases} 3\lambda\langle\phi^2\rangle + g^2\langle\chi^2\rangle \\ g^2\langle\phi^2\rangle + h_i^2\langle\sigma_i^2\rangle \\ h_i^2\langle\chi^2\rangle \end{cases} \tag{12}$$

for ϕ, χ, and σ_i, respectively. For the classical waves of f that we are dealing with, n_k corresponds to an adiabatic invariant of the waves. Formula (9) can be interpreted as a particle occupation number in the limit of large amplitude of the f field. As we will see below this occupation number spectrum contains important information about thermalization. Notice that the effective mass of the particles depends on the variances of the fields and may be significant and time dependent. The momenta of the particles do not necessarily always exceed their masses, meaning the interacting scalar waves are not necessarily always in the kinetic regime. In particular this means that in general we cannot calculate the energies of the fields simply as $\int d^3k\,\omega_k n_k$ because interaction terms between fields can be significant.

From here on we will use n without a subscript to denote the total number density for a field, and will use the subscript only to specify a particular field, e.g. n_ϕ. We use n_{tot} to mean the sum of the total number density for all fields combined. The occupation number will always be written n_k and it should be clear from context which field is being referred to.

In practice it is not very important whether you consider the spectrum f_k and the variance of f or the spectrum n_k and the number density. Both sets of quantities qualitatively show the same behavior in the systems we are considering. The variance and number density grow exponentially during preheating and evolve much more slowly during the subsequent stage of turbulence. Most of our results are shown in terms of number density n_f and occupation number n_k because these quantities have obvious physical interpretations, at least in certain limiting cases. We shall occasionally show plots of variance for comparison purposes.

We will follow the evolution of $n(t)$ and $n_k(t)$. The evolution of the total number density n_{tot} is an indication of the physical processes taking place. In the weak interaction limit the scattering of classical waves via the interaction term $\frac{1}{2}g^2\phi^2\chi^2$ can be treated using a perturbation expansion with respect to g^2. The leading four-leg diagrams for this interaction corresponds to a two-particle collision ($\phi\chi\rightarrow\phi\chi$), which conserves n_{tot}. The regime where such interactions dominate corresponds to ''weak turbulence'' in the terminology of the theory of wave turbulence [12]. If we see n_{tot} conserved, it will be an indication that these two-particle collisions constitute the dominant interaction. Conversely, violation of $n_{tot}(t)=$const will indicate the presence of strong turbulence, i.e., the importance of many-particle collisions. Such higher order interactions may be significant despite the smallness of the coupling parameter g^2 (and others) because of the large occupation numbers n_k. Later, when these occupation numbers are reduced by rescattering, the two-particle collision should become dominant and n_{tot} should be conserved.

For a bosonic field in thermal equilibrium with a temperature T and a chemical potential μ the spectrum of occupation numbers is given by

$$n_k = \frac{1}{e^{(\omega_k - \mu)/T} - 1}. \tag{13}$$

(We use units in which $\hbar=1$.) Preheating generates large occupation numbers for which Eq. (13) reduces to its classical limit

$$n_k \approx \frac{T}{\omega_k - \mu}, \tag{14}$$

which in turn reduces to $n_k \propto 1/k$ for $k \gg m, \mu$ and $n_k \approx$const for $k \ll m, \mu$. We will compare the spectrum n_k to this form to judge how the fields are thermalizing. Here we consider the chemical potential of an interacting scalar fields as a free parameter.

Unless otherwise indicated all of our results are shown in comoving coordinates that, in the absence of interactions,

would remain constant as the universe expanded. Note also that for most of our discussion we consider field spectra only as a function of $|\vec{k}|$, defined by averaging over spherical shells in k space. For a Gaussian field these spectra contain all the information about the field, and even for a non-Gaussian field most useful information is in these averages. This issue is discussed in more detail in Sec. V.

C. Results

The key results for this model are shown in Figs. 1–8, which show the evolution of $n(t)$ with time for each field and the spectrum n_k for each field at a time long after the end of preheating. These results are shown for runs with one field (ϕ only), two fields (ϕ and χ), and three and four fields (one and two σ_i fields respectively). We will begin by discussing some general features common to all of these runs and then comment on the runs individually.

All of the plots of $n(t)$ show an exponential increase during preheating, followed by a gradual decrease that asymptotically slows down. See for example Fig. 9. This exponential increase is a consequence of explosive particle production due to parametric resonance. This regime is fairly well understood [9]. After preheating the fields enter a turbulent regime, during which $n(t)$ decreases. This initial, fast decrease can be interpreted as a consequence of the many-particle interactions discussed above; as n_k shifts from low to high momenta the overall number decreases. Realistically, however, the onset of weak turbulence should be accompanied by the development of a compensating flow towards infrared modes, which we would be unable to see because of our finite box size. Thus the continued, slow decrease in $n(t)$ well into the weak turbulent regime is presumably a consequence of the lack of very long wavelength modes in our lattice simulations.

To see why this shift is occurring look at the spectra n_k (Figs. 5–8; see also [7,13]). Even long after preheating the infrared portions of some of these spectra are tilted more sharply than would be expected for a thermal distribution (14). Even more importantly, many of them show a cutoff at some momentum k, above which the occupation number falls off exponentially. Both of these features, the infrared tilt and the ultraviolet cutoff, indicate an excess of occupation number at low k relative to a thermal distribution. This excess occurs because parametric resonance is typically most efficient at exciting low momentum modes, and becomes completely inefficient above a certain cutoff k_*. A clear picture of how the flow to higher momenta reduces these features can be seen in Fig. 10, which shows the evolution of the spectrum n_k for χ in the two field model.

Figure 10 illustrates the initial excitation of modes in particular resonance bands, followed by a rapid smoothing out of the spectrum. The ultraviolet cutoff is initially at the momentum k_* where parametric resonance shuts down, but over time the cutoff moves to higher k as more modes are brought into the quasi-equilibrium of the infrared part of the spectrum. Meanwhile the infrared section is gradually flattening as it approaches a true thermal distribution. During preheating the excitation of the infrared modes drives this
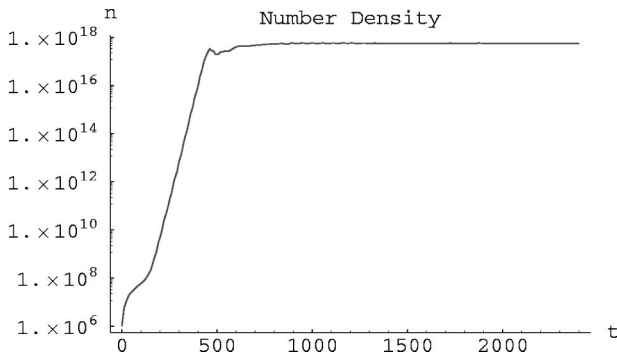
NUMBER DENSITY VS TIME

FIG. 1. $V = 1/4\lambda\phi^4$. (Note that the vertical scale is larger than for the subsequent plots.)
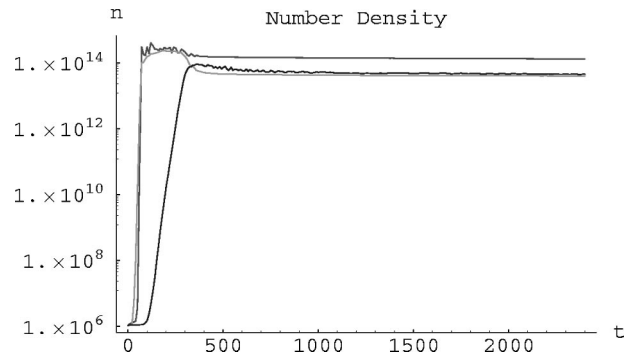

FIG. 3. $V = 1/4\lambda\phi^4 + 1/2g^2\phi^2\chi^2 + 1/2h^2\chi^2\sigma^2$, $g^2/\lambda = 200$, $h^2 = 100g^2$. The highest curve is n_ϕ. The number density of χ diminishes when n_σ grows.
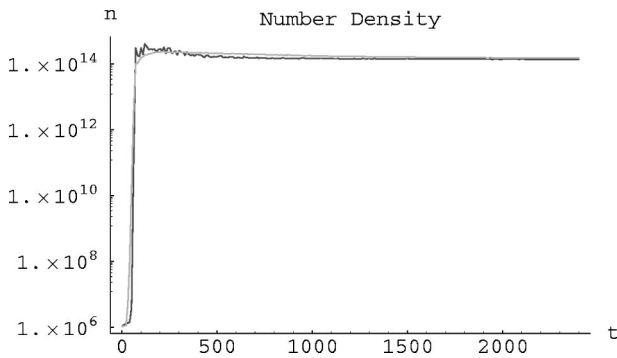

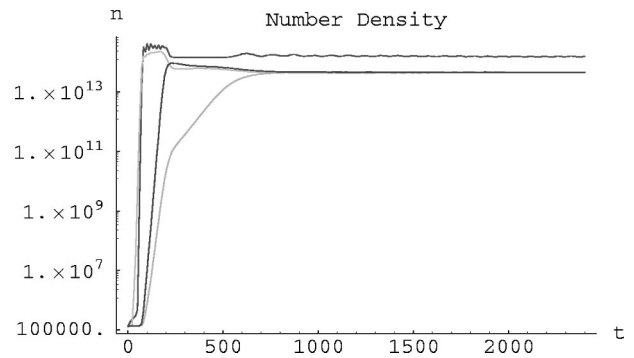FIG. 2. $V = 1/4\lambda\phi^4 + 1/2g^2\phi^2\chi^2$, $g^2/\lambda = 200$. The upper curve represents n_χ.

FIG. 4. $V = 1/4\lambda\phi^4 + 1/2g^2\phi^2\chi^2 + 1/2h_i^2\chi^2\sigma_i^2$, $g^2/\lambda = 200$, $h_1^2 = 200g^2$, $h_2^2 = 100g^2$. The pattern is similar to the three-field case until the growth of σ_2.

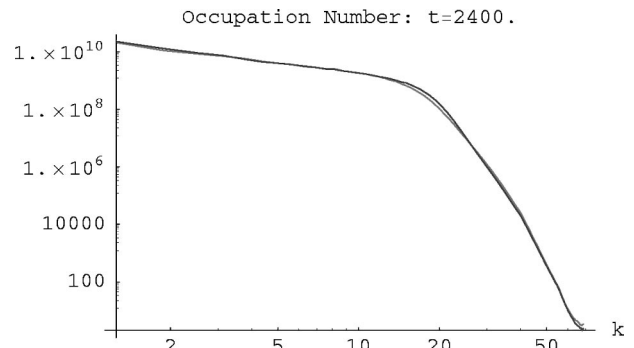## OCCUPATION NUMBER VS MOMENTUM
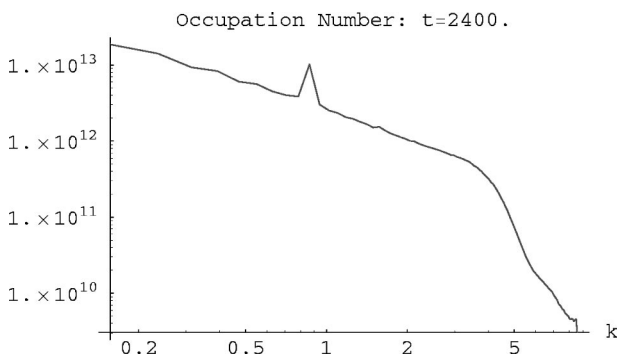
FIG. 5. $V = 1/4\lambda\phi^4$.

FIG. 6. $V = 1/4\lambda\phi^4 + 1/2g^2\phi^2\chi^2$, $g^2/\lambda = 200$. The spectra of ϕ and χ are nearly identical.
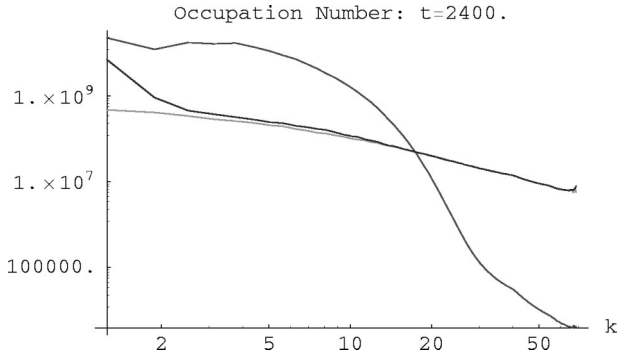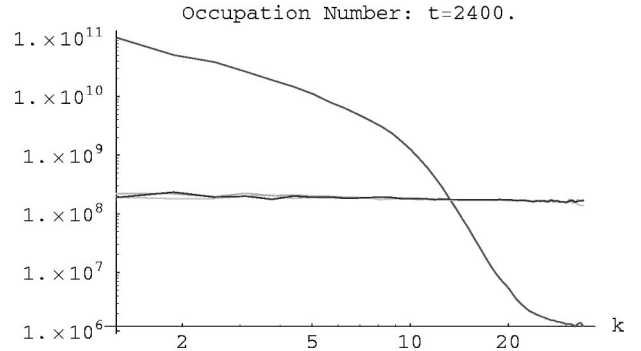
Occupation Number: t=2400.

FIG. 7. $V = 1/4\lambda\phi^4 + 1/2g^2\phi^2\chi^2 + 1/2h^2\chi^2\sigma^2$, $g^2/\lambda = 200$, $h^2 = 100g^2$. The χ and σ spectra are similar, but σ rises in the infrared. The spectrum of ϕ is markedly different from the others.

Occupation Number: t=2400.

FIG. 8. $V = 1/4\lambda\phi^4 + 1/2g^2\phi^2\chi^2 + 1/2h_i^2\chi^2\sigma_i^2$, $g^2/\lambda = 200$, $h_1^2 = 200g^2$, $h_2^2 = 100g^2$. All fields other than the inflaton have nearly identical spectra.

slope to large, negative values. From then on it gradually approaches thermal equilibrium (i.e., a slope of -1 to 0 depending on the chemical potential and the mass). The relaxation time for the equilibrium is significantly shorter than that given by formula $1/n\sigma_{int}$. This estimate is valid for dilute gases of particles, but in our case the large occupation numbers amplify the scattering amplitudes [4].

Figure 11 shows the evolution of the variances $\langle(f - \bar{f})^2\rangle$ for the two field model. As indicated above it shows all the same qualitative features as the evolution of n for that model.

We can now go on to point out some differences between the models, i.e., between runs with different numbers of fields. The one field model (pure $\lambda\phi^4$) shows the basic features discussed above, but the tilt in the spectrum is still very large at the end of the simulation and n_ϕ is decreasing very slowly compared to the spectral tilt and change in n we see in the two field case. This difference occurs because the interactions between ϕ and χ greatly speed up the thermalization of both fields. In the one field case ϕ can only thermalize via its relatively weak self-interaction.

The spectra in the two field run also show a novel feature, namely that the spectra for ϕ and χ are essentially identical, which means, among other things,

$$n_\phi \approx n_\chi. \tag{15}$$

This matching of the two spectra occurs shortly after preheating and from then on the two fields evolve identically (except for the remaining homogeneous component of ϕ). *A posteriori* this result can be understood as follows. Looking at the potential $\lambda\phi^4 + g^2\phi^2\chi^2$, the second term dominates because of the hierarchy of coupling strengths $g^2 = 200\lambda$. So the potential $V \approx g^2\phi^2\chi^2$ is symmetric with respect to the two fields, and therefore they act as a single effective field.

Figures 3 and 7 show the effects of adding an additional decay channel for χ. The interaction of χ and σ does not affect the preheating of χ, but does drag σ exponentially quickly into an excited state. The field σ is exponentially amplified not by parametric resonance, but by its stimulated interactions with the amplified χ field. Unlike amplification by preheating, this direct decay nearly conserves particle number, with the result that n_χ decreases as σ grows, and the spectra of ϕ and χ are no longer identical. Instead χ and σ develop nearly identical spectra,
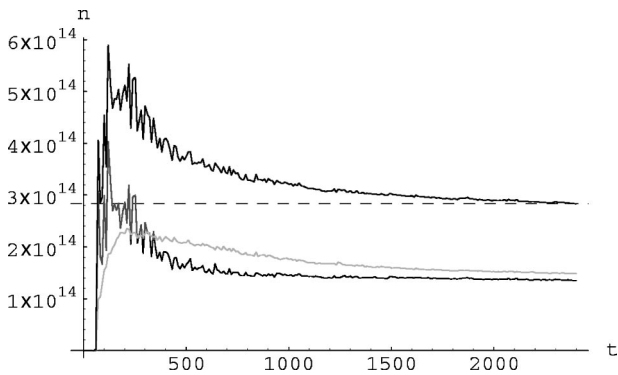
$$n_\chi \approx n_\sigma < n_\phi, \tag{16}$$

FIG. 9. Number density n for $V = \frac{1}{4}\lambda\phi^4 + \frac{1}{2}g^2\phi^2\chi^2$. The plots are, from bottom to top at the right of the figure, n_ϕ, n_χ, and n_{tot}. The dashed horizontal line is simply for comparison. The end of exponential growth and the beginning of turbulence (i.e., the moment t_*) occurs around the time when n_{tot} reaches its maximum.
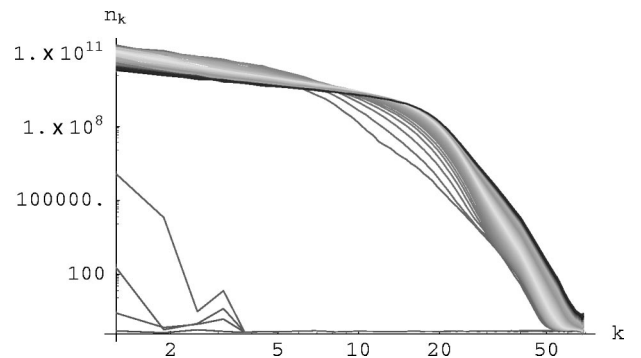

FIG. 10. Evolution of the spectrum of χ in the model $V = \frac{1}{4}\lambda\phi^4 + \frac{1}{2}g^2\phi^2\chi^2$. Red plots correspond to earlier times and blue plots to later ones. For black and white viewing: The sparse, lower plots all show early times. In the thick bundle of plots higher up the spectrum is rising on the right and falling on the left as time progresses.
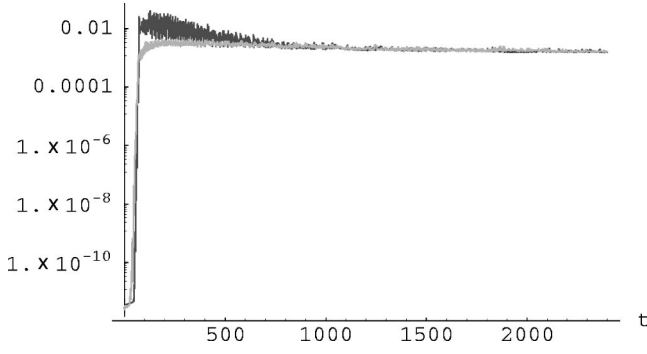
FIG. 11. Variances for $V = \frac{1}{4}\lambda\phi^4 + \frac{1}{2}g^2\phi^2\chi^2$. The upper plot shows $\langle(\phi - \bar{\phi})^2\rangle$ and the lower plot shows $\langle(\chi - \bar{\chi})^2\rangle$.

and they both thermalize (together) much more rapidly than χ did in the absence of σ. There is a looser relationship $n_\phi \approx n_\sigma + n_\chi$, whose accuracy depends on the couplings. The inflaton, meanwhile, thermalizes much more slowly; note the low k of the cutoff in the ϕ spectrum in Fig. 7. By contrast, there is no visible cutoff in the spectra of χ and σ and the tilt is relatively mild. The most striking property of this chain of interaction is the grouping of fields; χ and σ behave identically to each other and differently from ϕ. This again can be understood by the hierarchy of coupling constants, $h^2 = 100g^2 = 20\,000\lambda$. The term $h^2\chi^2\sigma^2$ is dominant and puts χ and σ on an equal footing.

Varying the coupling h did not change the overall behavior of the system, but it changed the time at which σ grew. In the limiting case $h \gg g$, σ grew with χ during preheating and remained indistinguishable from it right from the start. (We found this, for example, for $h^2 = 10\,000g^2$.)

When we added a second σ field we found that the σ field most strongly coupled to χ would grow very rapidly and the more weakly coupled one would then grow relatively slowly. Note for example that $n_{\sigma 2}$ in Fig. 8 grows more slowly than n_σ in Fig. 7 despite the fact that they have the same coupling to χ. In the four field case n_χ is reduced when the more strongly coupled σ field grows and this slows the growth of the more weakly coupled one. Nonetheless, the addition of
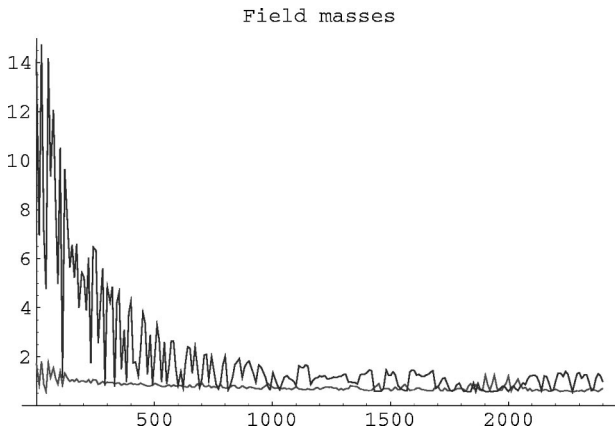

FIG. 12. Effective masses for $V = \frac{1}{4}\lambda\phi^4 + \frac{1}{2}g^2\phi^2\chi^2$ as a function of time in units of comoving momentum. The lower plot is m_ϕ and the upper one is m_χ.
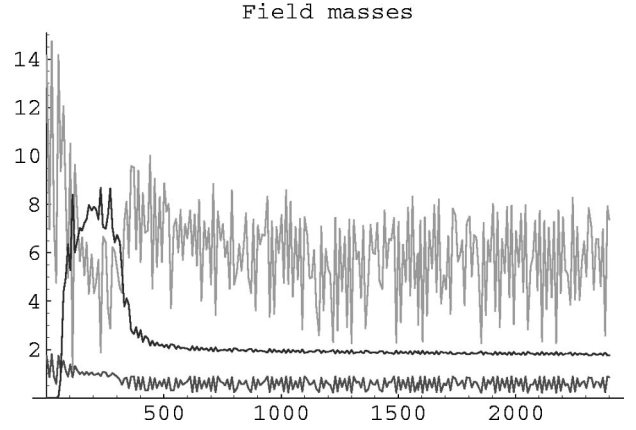

FIG. 13. Time evolution of the effective masses for the model $V = \frac{1}{4}\lambda\phi^4 + \frac{1}{2}g^2\phi^2\chi^2 + \frac{1}{2}h^2\chi^2\sigma^2$. From bottom to top on the right hand side the plots show m_ϕ, m_σ, and m_χ.

another σ field once again sped up the thermalization of χ and the σ fields. The three fields χ, σ_1, and σ_2 once again have identical spectra

$$n_\chi \approx n_{\sigma 1} \approx n_{\sigma 2} < n_\phi, \tag{17}$$

but in the four field case by the end of the run they look indistinguishable from thermal spectra. If there is an ultraviolet cutoff for these spectra, it is at momenta higher than can be seen on the lattice we were using. Again, we notice a loose relationship $n_\phi \approx n_\chi + n_{\sigma 1} + n_{\sigma 2}$. in this case.

We close this section with a few words about the effective masses of the fields, Eq. (11). All the masses are scaled in the comoving frame; i.e., we consider $a^2 m_{eff}^2$, and m is measured in units of momentum (see the Appendix). Figure 12 shows the evolution of the effective masses in the two field model. Note that the vertical axis of these plots is in the same comoving units as the horizontal (k) axes of the spectra plots. Since the momentum cutoff was of order $k \sim 5-10$ (see Fig. 10) the mass of ϕ was consistently smaller than the typical momenta of the field. By contrast m_χ started out much larger and only gradually decreased. The fluctuations of χ remained massive through preheating (although with a physical mass $\sim 1/a$) and for quite a while afterwards the typical momentum of these fluctuations was $k \sim m$.

Figure 13 shows the evolution of the effective masses for the three field model. Once again m_ϕ remains small. Although m_σ grows large briefly it quickly subsides. However, m_χ, with contributions from σ and ϕ, remains relatively large. Note, however, that the spectrum of χ has no clear cutoff after σ has grown, so it is difficult to say whether this mass exceeds a ''typical'' momentum scale or not.

IV. OTHER MODELS OF INFLATION AND INTERACTIONS

The model (3) was chosen to illustrate our basic results because $\lambda\phi^4$ inflation and preheating is relatively simple and well studied. Our main interest, however, is in universal features of thermalization. In this section we therefore more briefly discuss our results for a variety of other models. First

we continue with $\lambda\phi^4$ inflation by discussing variants on the interaction potential described above. Next we discuss thermalization in $m^2\phi^2$ models of chaotic inflation. Finally we discuss hybrid inflation.

A. Variations of chaotic inflation with a quartic potential

We looked at several simple variants of the potential (3). We considered a model with a further decay channel for σ so that the total potential was

$$V=\frac{1}{4}\lambda\phi^4+\frac{1}{2}g^2\phi^2\chi^2+\frac{1}{2}h_1^2\chi^2\sigma^2+\frac{1}{2}h_2^2\sigma^2\gamma^2. \quad (18)$$

Setting $h_1=h_2$ we found that for this four field model the evolution of the field fluctuations, spectra, and number density were qualitatively similar to those in the four field model (3). We found that at late times

$$n_\chi\approx n_\sigma\approx n_\gamma < n_\phi. \quad (19)$$

The fields χ, σ, and γ formed a group with nearly identical spectra and evolution and rapid thermalization, while ϕ remained distinct and thermalized more slowly. Compare these results to the four field model results in Figs. 4 and 8.

We also considered parallel decay channels for ϕ:

$$V=\frac{1}{4}\lambda\phi^4+\frac{1}{2}g_1^2\phi^2\chi^2+\frac{1}{2}g_2^2\phi^2\gamma^2+\frac{1}{2}h^2\chi^2\sigma^2. \quad (20)$$

Setting $g_1=g_2$ and $h^2=100g_1^2$ we found that, at late times,

$$n_\phi\approx n_\gamma > n_\chi\approx n_\sigma. \quad (21)$$

In other words the four fields formed into two groups of two, with each group having a characteristic number density evolution.

Finally we looked at adding a self-interaction term for χ,

$$V=\frac{1}{4}\lambda_\phi\phi^4+\frac{1}{2}g^2\phi^2\chi^2+\frac{1}{4}\lambda_\chi\chi^4 \quad (22)$$

with $\lambda_\chi=g^2$, and found that the results were essentially unchanged from those of the two field runs with no χ^4 term. The χ self-coupling caused the spectra of ϕ and χ to deviate slightly from each other, but their overall evolution proceeded very similarly to the case with no χ self-interaction term.

B. Chaotic inflation with a quadratic potential

We also considered chaotic inflation models with an $m^2\phi^2$ inflaton potential. Figures 14–17 show results for the model

$$V=\frac{1}{2}m^2\phi^2+\frac{1}{2}g^2\phi^2\chi^2+\frac{1}{2}h^2\chi^2\sigma^2, \quad (23)$$

with $m=10^{-6}M_p\approx1.22\times10^{13}$ GeV (for COBE), $g^2=2.5\times10^5m^2/M_p^2$, and $h^2=100g^2$. (See the Appendix for more details.) We considered separately the case of two fields ϕ and χ and three fields ϕ, χ, and σ. This model exhibits

parametric resonance similar to the resonance in quartic inflation [4], which results in the rapid growth of n seen in these figures. The spectra produced in this way are once again tilted towards the infrared. In the two field case, ϕ and χ do not have identical spectra as they did for quartic inflation. This is because the coupling term $1/2g^2\phi^2\chi^2$ redshifts more rapidly than the mass term $1/2m^2\phi^2$, so the latter remains dominant in the potential, which is therefore not symmetric between ϕ and χ. In the three field case we again see similar spectra for χ and σ, although they are not as indistinguishable as they were in $\lambda\phi^4$ theory. The basic features of rapid growth of n, high occupation of infrared modes, and then a flux of number density towards ultraviolet modes and a slow decrease in n_{tot} are all present as they were for $\lambda\phi^4$ theory. The shape of the ϕ spectrum does not appear thermal, but it is unclear if this spectrum is compatible with Kolmogorov turbulence.

C. Hybrid inflation

Preheating has been studied in many different versions of hybrid inflation, mostly only at the early stages when the equations for the fluctuations can be linearized. It had been thought until recently that preheating was not a universal process in hybrid inflation. In our recent study [5], however, we found that there is generally a very strong preheating in hybrid models, but its character is quite different from preheating based on parametric resonance. We discuss in detail in a separate publication [5] our recent analytical and numerical studies of preheating in hybrid inflation models, including a simple two-field model (2) as well as more complex supersymmetric (SUSY) F-term and D-term models. As with parametric resonance, the result of the instability is the exponential growth of long-wavelength modes of the fields.

In this paper we are mostly interested in preheating in the non-inflaton sector and the nonlinear stage after preheating. In [5] we studied the instability in the inflaton sector of the hybrid model, i.e., the decay of the homogeneous fields and excitations of their fluctuations. Here we take a complementary approach and consider the dynamics of the model with an additional scalar field χ coupled to the fields of the hybrid inflation model. The potential is

$$V=\frac{\lambda}{4}|4\bar{\Sigma}\Sigma-v^2|^2+4\lambda|\Phi|^2(|\Sigma|^2+|\bar{\Sigma}|^2)+h^2\chi^2|\Sigma|^2, \quad (24)$$

where $\lambda=2.5\times10^{-5}$ and $h^2=2\lambda$. Here Φ, Σ and $\bar{\Sigma}$ are the complex scalar fields of the inflaton sector and χ is an additional matter field. Inflation occurs along of the Φ direction for $\langle\Phi\rangle\gg v$, when $\Sigma=\bar{\Sigma}=0$. When the magnitude of the slow-rolling field Φ reaches the value $\langle|\Phi_c|\rangle=v/2$ spontaneous symmetry breaking occurs and the Σ fields become excited. It can be shown that at the end of inflation and the start of symmetry breaking the complicated potential (24) can be effectively reduced to the simple two field potential (2) (where ϕ and σ are combinations of Φ, Σ, $\bar{\Sigma}$ and $g^2=\frac{1}{2}\lambda$) plus the coupling term with $h^2\chi^2|\Sigma|^2$.

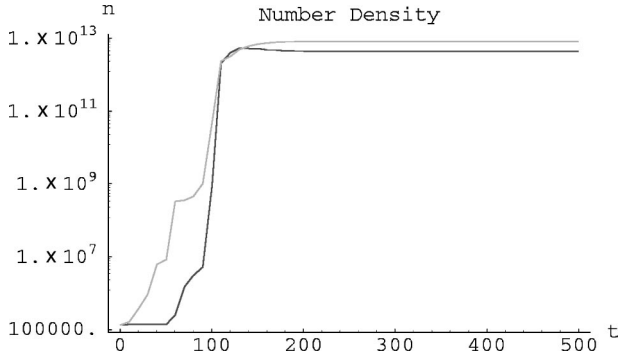## NUMBER DENSITY VS TIME

FIG. 14. $V = 1/2m^2\phi^2 + 1/2g^2\phi^2\chi^2$, $g^2M_p^2/m^2 = 2.5\times10^5$. The upper curve represents n_χ.
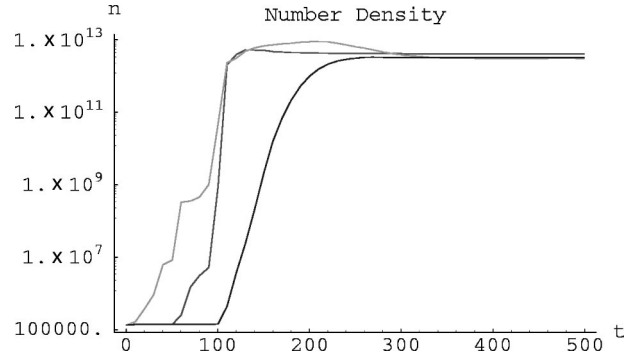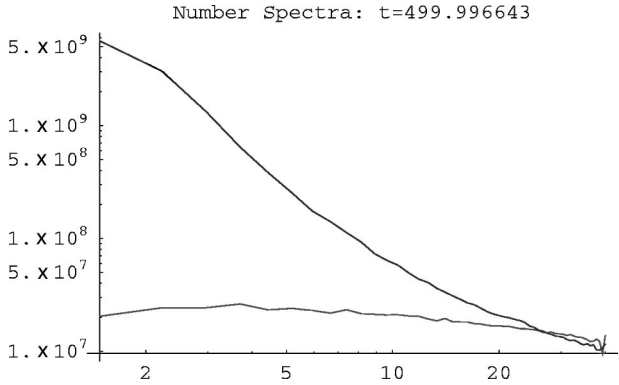

FIG. 15. $V = 1/2m^2\phi^2 + 1/2g^2\phi^2\chi^2 + 1/2h^2\chi^2\sigma^2$, $g^2M_p^2/m^2 = 2.5\times10^5$, $h^2 = 100g^2$. The highest curve is n_χ. The field that grows the latest is σ.

NUMBER DENSITY VS MOMENTUM

FIG. 16. $V = 1/2m^2\phi^2 + 1/2g^2\phi^2\chi^2$, $g^2M_p^2/m^2 = 2.5\times10^5$. The upper curve represents the spectrum of χ.
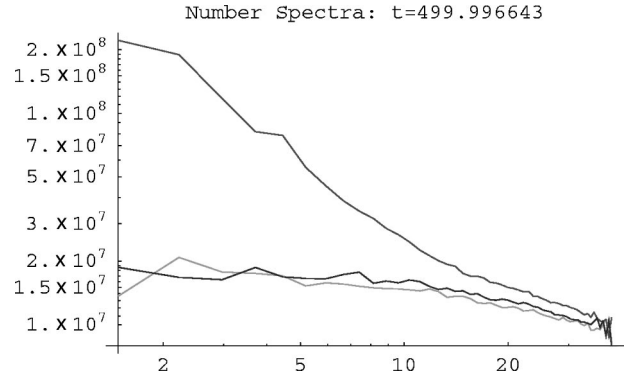

FIG. 17. $V = 1/2m^2\phi^2 + 1/2g^2\phi^2\chi^2 + 1/2h^2\chi^2\sigma^2$, $g^2M_p^2/m^2 = 2.5\times10^5$, $h^2 = 100g^2$. The χ and σ spectra are similar, while the spectrum of ϕ rises much higher in the infrared.

Figure 18 shows the evolution of the six degrees of freedom of the inflaton sector as well as the field χ. We see that all of the inflaton fields except $\text{Im}(\Phi)$ are excited very quickly. Later the fields χ and $\text{Im}(\Phi)$ are dragged into excited states as well. This dragging corresponds to preheating in the non-inflaton sector. The fields χ and $\text{Im}(\Phi)$ are excited by their stimulated interactions with the rest of the fields. The result of this amplification is a turbulent state that evolves towards equilibrium very similarly to the chaotic models. Although the details of inflation and preheating are very different in hybrid and chaotic models, we found that once a matter field has been amplified, the thermalization process proceeds in the same way.

V. ONSET OF CHAOS, LYAPUNOV EXPONENTS AND STATISTICS

Interacting waves of scalar fields constitute a dynamical system, meaning there is no dissipation and the system can be described by a Hamiltonian. Dynamical chaos is one of

the features of wave turbulence. In this section we address the question if, how and when the onset of chaos takes place after preheating.

The scalar field fluctuations produced during preheating are generated in squeezed states [14,4] that are characterized by correlations of phases between modes $\vec{k}$ and $-\vec{k}$. Because of their large amplitudes, we can consider these fluctuations to be standing classical waves with definite phases. During the linear stage of preheating, before interactions between modes become significant, the evolution of these waves may be or may not show chaotic sensitivity to initial conditions. Indeed, for wide ranges of coupling parameters parametric resonance has stochastic features [4,9], and the issue of the numerical stability of parametric resonance has not been investigated. When interaction (rescattering) between waves becomes important, the waves become decoherent. At this stage the waves have well-defined occupation numbers but not well-defined phases, and the random phase approximation can be used to describe the system. This transition sig-
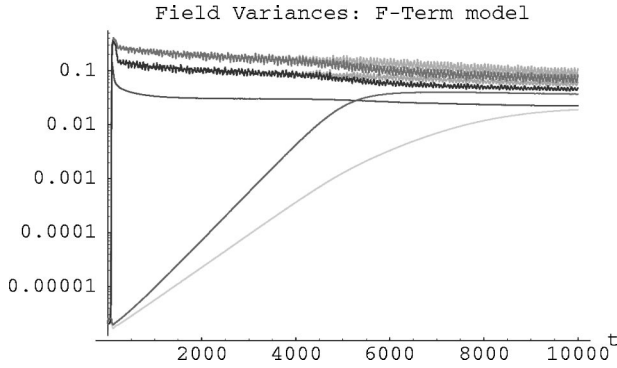
FIG. 18. Evolution of variances of fields in the model (24). The two fields that grow at late times, in order of their growth, are χ and $\text{Im}(\Phi)$.

nals the onset of turbulence, following which the system will gradually evolve towards thermal equilibrium.

To investigate the onset of chaos in this system we have to follow the time evolution of two initially nearby points in the phase space; see e.g. [8]. Consider two configurations of a scalar field f and f' that are identical except for a small difference of the fields at a set of points x_A. We use $f(t,\vec{x}_A), \dot{f}(t,\vec{x}_A)$ to indicate the unperturbed field amplitude and field velocity at the point $\vec{x}_A$ and $f'(t,\vec{x}_A), \dot{f}'(t,\vec{x}_A)$ to indicate slightly perturbed values at this point. In other words, the field configurations with $f(t,\vec{x}_A), \dot{f}(t,\vec{x}_A)$ and $f'(t,\vec{x}_A), \dot{f}'(t,\vec{x}_A)$ are initially close points in the field phase space. We then independently evolve these two systems (phase space points) and observe how the perturbed field values diverge from the unperturbed ones. Chaos can be defined as the tendency of such nearby configurations in phase space to diverge exponentially over time. This divergence is parametrized by the Lyapunov exponent for the system, defined as

$$\lambda \equiv \frac{1}{t}\log\frac{D(t)}{D_0} \qquad (25)$$

where D is a distance between two configurations and D_0 is the initial distance at time 0. Here we define the distance $D(t)$ simply as
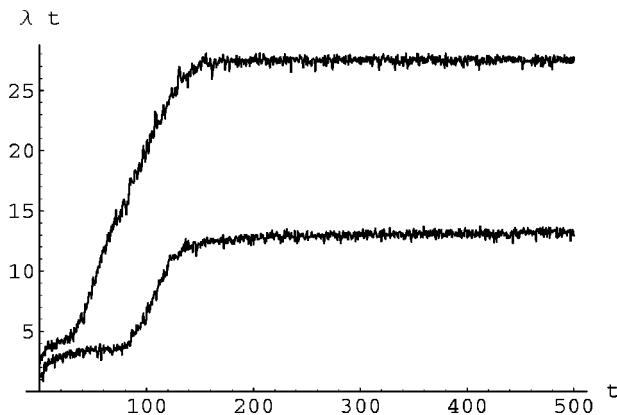

FIG. 19. The Lyapunov exponent λ for the fields ϕ (lower curve) and χ (upper curve). The vertical axis is λt.
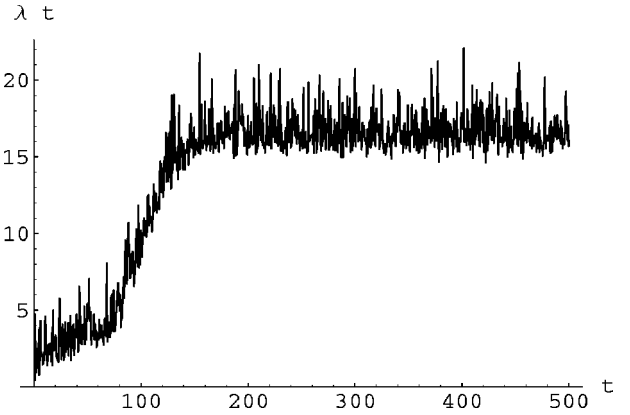

FIG. 20. The Lyapunov exponent λ' for the fields ϕ and χ using the normalized distance function Δ.

$$D(t)^2 \equiv \sum_A \ (|f'_A-f_A|)^2 + (|\dot{f}'_A-\dot{f}_A|)^2, \qquad (26)$$

where we define $f_A \equiv f(t,\vec{x}_A)$ and the summation is taken over all the points where the configurations initially differed.

For illustration we present the calculations for the model $V = \frac{1}{4}\lambda\phi^4 + \frac{1}{2}g^2\phi^2\chi^2$. We did two lattice simulations of this model with initial conditions that were identical except that in one of them we multiplied the amplitude of χ by 1 $+10^{-6}$ at 8 evenly spaced points on the lattice. Figure 19 shows the Lyapunov exponent for both fields ϕ and χ. Note that the vertical axis is λt rather than just λ. During the turbulent stage the parameter $D(t)$ is artificially saturated to a constant because of the limited phase space volume of the system. Fortunately, the most interesting moment around t_*, where the chaotic motion begins, is covered by this simple approach. Certainly, the field dynamics continue to be chaotic in subsequent stages of the turbulence, and one can use more sophisticated methods to calculate the Lyapunov exponent during these stages [15,8]. However, this issue is less relevant for our study.

Both fields show roughly the same rate of growth of λ, but λ_χ grows much earlier than λ_ϕ and therefore reaches a higher level. The reason for this is simple. The amplitude of χ is initially very small and grows exponentially, so even in the absence of chaos we would expect that during preheating the difference $\chi'(t,\vec{x}_A) - \chi(t,\vec{x}_A)$ must grow exponentially, proportionally to $\chi \sim \exp[\int dt \mu(t)]$ itself. So this exponential growth is not a true indicator of chaos.

To get around this problem and define the onset of chaos in the context of preheating more meaningfully we introduce a normalized distance function

$$\Delta(t) \equiv \sum_A \left(\frac{f'_A-f_A}{f'_A+f_A}\right)^2 + \left(\frac{\dot{f}'_A-\dot{f}_A}{\dot{f}'_A+\dot{f}_A}\right)^2, \qquad (27)$$

which is well regularized even while the field χ is being amplified exponentially. Figure 20 shows the Lyapunov exponent
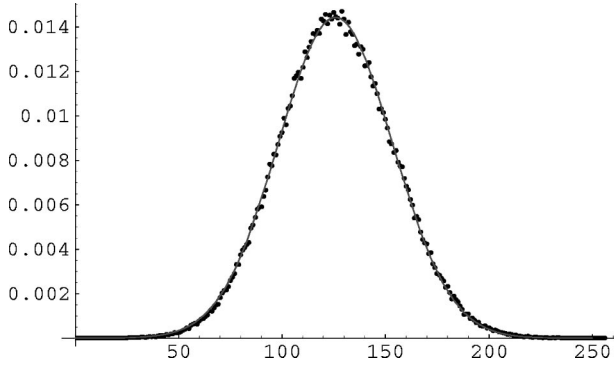
FIG. 21. The probability distribution function for the field χ after preheating. Dots show a histogram of the field and the solid curve shows a best-fit Gaussian.

$$\lambda' \equiv \frac{1}{t} \log \frac{\Delta(t)}{\Delta(t_0)}$$

for χ. In this case we see the onset of chaos only at the end of preheating. The plot for the ϕ field is nearly identical. The Lyapunov exponents for the fields were $\lambda'_\phi \approx \lambda'_\chi \approx 0.2$ (in the units of time adopted in the simulation). This corresponds to a very fast onset of chaos.

Thus we see that chaotic turbulence starts abruptly at the end of preheating. Initially wave turbulence is strong and rescattering does not conserve the total number of particles n_{tot}. The fastest variation in n_{tot} occurs at the same time as the onset of chaos, $t_* \sim 100-200$. We conjecture that the entropy of the system of interacting waves is generated around the moment t_*. As the particle occupation number drops, the turbulence will become weak and n_{tot} will be conserved. Figure 9 clearly shows this evolution of the total number of particles n_{tot} in the model.

We also considered the statistical properties of the interacting classical waves in the problem. The initial conditions of our lattice simulations correspond to random Gaussian noise. In thermal equilibrium, the field velocity $\dot{f}$ has Gaussian statistics, while the field f itself departs from that unless it has high occupation numbers. Figure 21 shows the probabil-
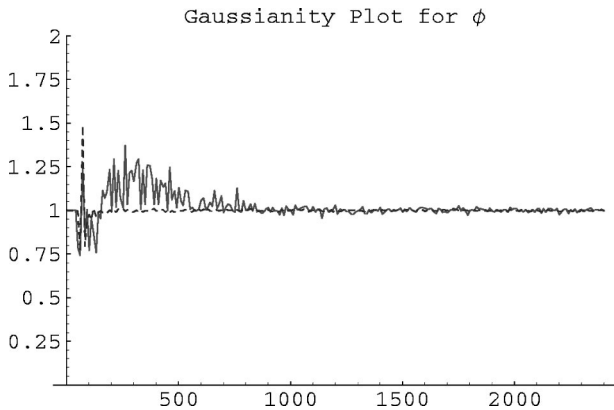

FIG. 22. Deviations from Gaussianity for the field ϕ as a function of time. The solid line shows $3\langle \delta\phi^2 \rangle^2 / \langle \delta\phi^4 \rangle$ and the dashed line shows $3\langle \delta\dot{\phi}^2 \rangle^2 / \langle \delta\dot{\phi}^4 \rangle$.
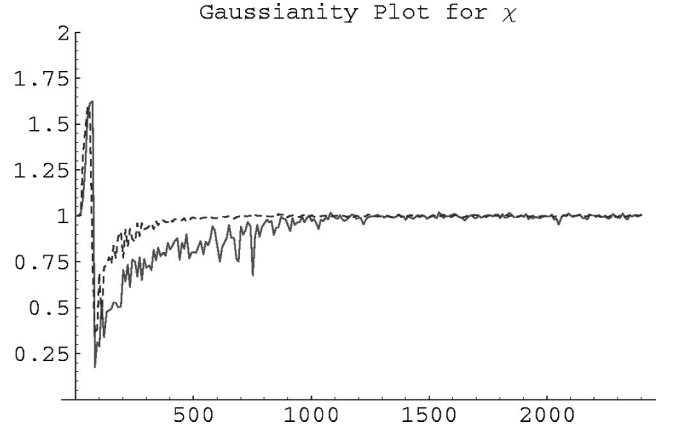

FIG. 23. Deviations from Gaussianity for the field χ as a function of time. The solid line shows $3\langle \delta\chi^2 \rangle^2 / \langle \delta\chi^4 \rangle$ and the dashed line shows $3\langle \delta\dot{\chi}^2 \rangle^2 / \langle \delta\dot{\chi}^4 \rangle$.

ity distribution of the field χ during the weak turbulence stage after preheating, and indeed the distribution is nearly exactly Gaussian. Thus, at this stage we can treat the superposition of classical scalar waves with large occupation numbers and random phases as random Gaussian fields.

During preheating, however, this Gaussian distribution is altered. A simple measure of the Gaussianity of a field comes from examining its moments. For a Gaussian field there is a fixed relationship between the two lowest nonvanishing moments, namely

$$3\langle \delta\phi^2 \rangle^2 = \langle \delta\phi^4 \rangle, \qquad (28)$$

where $\delta\phi \equiv \phi - \langle \phi \rangle$ and angular brackets denote ensemble averages or, equivalently, large spatial averages. We measured the ratio of the left and right hand sides of this equation for ϕ and χ and their time derivatives using spatial averages over the lattice. The results are shown in Figs. 22 and 23. As expected, the fields are initially Gaussian, deviate from it during preheating, and rapidly return to it afterwards. The plots for the moments of the field velocities are similar, although the field velocities remain closer to Gaussianity.

It is quite important to notice that Gaussianity is broken around the end of preheating and the beginning of the strong turbulence. In particular, it makes invalid the use of the Hartree approximation beyond this point.

VI. RULES OF THERMALIZATION

This paper is primarily an empirical one. We have numerically investigated the processes of preheating and thermalization in a variety of models and determined a set of rules that seem to hold generically. These rules can be formulated as follows:

(1) In many, if not all viable models of inflation there exists a mechanism for exponentially amplifying fluctuations of at least one field χ. These mechanisms tend to excite long-wavelength excitations, giving rise to a highly infrared spectrum.

The mechanism of parametric resonance in single-field models of inflation has been studied for a number of years.

Contrary to the claims of some authors, this effect is quite robust. Adding additional fields (e.g. our σ fields) or self-couplings (e.g. χ^4) has little or no effect on the resonant period. Moreover, in many hybrid models a similar effect occurs due to other instabilities. The qualitative features of the fields arising from these processes seem to be largely independent of the details of inflation or the mechanisms used to produce the fields.

(2) Exciting one field χ is sufficient to rapidly drag all other light fields with which χ interacts into a similarly excited state.

We have seen this effect when multiple fields are coupled directly to χ and when chains of fields are coupled indirectly to χ. All it takes is one field being excited to rapidly amplify an entire sector of interacting fields. These second generation amplified fields will inherit the basic features of the χ field; i.e., they will have spectra with more energy in the infrared than would be expected for a thermal distribution.

(3) The excited fields will be grouped into subsets with identical characteristics (spectra, occupation numbers, effective temperatures) depending on the coupling strengths.

We have seen this effect in a variety of models. For example in the models (3) and (18) the χ and σ fields formed such a group. In general, fields that are interacting in a group such as this will thermalize much more quickly than other fields, presumably because they have more potential to interact and scatter particles into high momentum states.

(4) Once the fields are amplified, they will approach thermal equilibrium by scattering energy into higher momentum modes.

This process of thermalization involves a slow redistribution of the particle occupation number as low momentum particles are scattered and combined into higher momentum modes. The result of this scattering is to decrease the tilt of the infrared portion of the spectrum and increase the ultraviolet cutoff of the spectrum. Within each field group the evolution proceeds identically for all fields, but different groups can thermalize at very different rates.

VII. DISCUSSION

We investigated the dynamics of interacting scalar fields during post-inflationary preheating and the development of equilibrium immediately after preheating. We used three dimensional lattice simulations to solve the non-linear equations of motion of the classical fields.

There are a number of problems both from the point of view of realistic models of early universe preheating and from the point of view of non-equilibrium quantum field theory that we have not so far addressed. In this section we shall discuss some of them.

Although we considered a series of models of inflation and interactions, we mostly restricted ourselves to four-leg interactions. (The sole exception was the hybrid inflation model, which develops a three-leg interaction after symmetry breaking.) This meant that we still had a residual homogeneous or inhomogeneous inflaton field. In realistic models of inflation and preheating we expect the complete decay of the inflaton field. (There are radical suggestions to use the

residuals of the inflaton oscillations as dark matter or quintessence, but these require a great deal of fine tuning.) The problem of residual inflaton oscillations can be easily cured by three-leg interactions. In the scalar sector three-leg interactions of the type $g^2 v \phi \chi^2$ may result in stronger preheating. Yukawa couplings $h\bar{\psi}\phi\psi$ will lead to parametric excitations of fermions [16].

There are subtle theoretical issues related to the development of precise thermal equilibrium in quantum and classical field theory due to the large number of degrees of freedom; see, e.g., [17]. In our simulations we see the flattening of the particle spectra n_k and we describe this as an approach to thermal equilibrium, but in light of these subtleties we should clarify that we mean *approximate* thermal equilibrium.

Often classical scalar fields in the kinetic regime display transient Kolmogorov turbulence, with a cascade towards both infrared and ultraviolet modes [12,18]. In our systems it appears that the flux towards ultraviolet modes is occurring in such a way as to bring the fields closer to thermal equilibrium (14). Indeed, the slope of the spectra n_k at the end of our simulations is close to -1. However, given the size of the box in these simulations we can little say about the phase space flux in the direction of infrared modes. This question could be addressed, for example, with the complementary method of chains of interacting oscillators; see [18]. This is an interesting problem because an out-of-equilibrium Bose system of interacting scalars with a conserved number of particles can, in principle, develop a Bose condensate. It would be interesting to see how the formation of this condensate would or would not take place in the context of preheating in an expanding universe. One highly speculative possibility is that a cosmological Bose condensate could play the role of a late-time cosmological constant.

The highlights of our study for early universe phenomenology are the following. The mechanism of preheating after inflation is rather robust and works for many different systems of interacting scalars. There is a stage of turbulent classical waves where the initial conditions for preheating are erased. Initially, before all the fields have settled into equilibrium with a uniform temperature, the reheating temperature may be different in different subgroups of fields. The nature of these groupings is determined by the coupling strengths.

APPENDIX: THE LATTICE CALCULATIONS

All of the numerical calculations reported here were produced with the program LATTICEEASY, developed by Gary

Felder and Igor Tkachev.[1] In this appendix we merely summarize the basics of the calculation; more details can be found on the website. All quantities are measured in Planck units ($M_p \approx 1.22 \times 10^{19}$ GeV) and we use f to denote a generic scalar field.

The equations of motion for the fields and the scale factor a are solved on a three-dimensional lattice using finite differencing for spatial derivatives and a second-order staggered leapfrog algorithm for time evolution. The evolution equation for a scalar field in an expanding universe is

$$\ddot{f} + 3\frac{\dot{a}}{a}\dot{f} - \frac{1}{a^2}\nabla^2 f + \frac{\partial V}{\partial f} = 0 \qquad (A1)$$

while the evolution of the scale factor is given by the Friedmann equations

$$\left(\frac{\dot{a}}{a}\right)^2 = \frac{8\pi}{3}\rho \qquad (A2)$$

$$\ddot{a} = -\frac{4\pi}{3}(\rho + 3p)a \qquad (A3)$$

where the energy density and pressure of a scalar field are given by

$$\rho = \frac{1}{2}\dot{f}^2 + \frac{1}{2}|\nabla f|^2 + V \qquad (A4)$$

$$p = \frac{1}{2}\dot{f}^2 - \frac{1}{6}|\nabla f|^2 - V. \qquad (A5)$$

In a leapfrog scheme the field values and derivatives are known at different times, so it is convenient to combine Eqs. (A2) and (A3) to eliminate the field derivatives, giving

$$\ddot{a} = -2\frac{\dot{a}^2}{a} + \frac{8\pi}{3}\left(\frac{1}{3}|\nabla f|^2 - a^2 V\right), \qquad (A6)$$

where the gradient is summed over all fields.

The initial conditions were set in momentum space and then Fourier transformed to give the initial field values on the grid. Starting at the end of inflation we gave each mode a random phase and a Gaussian distributed amplitude with rms value

$$\langle |f_k|^2 \rangle = \frac{1}{\sqrt{2\omega_k}} \qquad (A7)$$

where

---

[1]The program and documentation are available on the web at http://physics.stanford.edu/gfelder/latticeeasy/ The site also includes all the files needed to implement the particular models discussed in this paper so anyone can easily reproduce our results.

$$\omega_k^2 = k^2 + m^2 = k^2 + \frac{\partial^2 V}{\partial f^2}. \qquad (A8)$$

In simulations it is useful to use energy conservation as a check of accuracy. Energy conservation in an expanding universe is described by the equation

$$\dot{\rho} + 3\frac{\dot{a}}{a}(\rho + p) = 0. \qquad (A9)$$

In principle one could verify that this equation was being satisfied during the run, but in practice $\dot{\rho}$ is more difficult to evaluate than ρ. Fortunately there is another way to accomplish the same thing. Equation (A9) can be derived from the two Friedmann equations (A2) and (A3), so checking that those two equations are being simultaneously satisfied is equivalent to checking Eq. (A9). Since the actual equation for the evolution of the scale factor is a combination of these two Friedmann equations, we were able to check energy conservation by calculating the ratio of $\dot{a}/a$ to $(8\pi/3)\rho$ as the program progressed. [We verified that checking Eq. (A3) gave the same results.] For the $\lambda\phi^4$ runs the theory is nearly conformal, so almost the same behavior is obtained with or without the expansion of the universe (if one uses conformal variables). So we duplicated a number of our runs without expansion and directly checked energy conservation. In all cases the results of these two methods of checking our accuracy were nearly identical. In every run we did, including cases where we did the run with and without expansion, energy was conserved to within half a percent over the entire run.

We also did a number of trials to ensure that our results were not sensitive to our time step, box size, or number of gridpoints.

The field equations were simplified by variable redefinitions. The redefinitions used and the resulting field equations for the chaotic inflation models described in the paper are given below. (Details on the hybrid inflation model can be found in [5].) The units for the fields, times, and momenta in all the plots in the paper are measured in Planck units rescaled as indicated below. Before these rescalings, time was in physical units and distances in comoving coordinates. The momenta k are also measured in comoving coordinates and they are changed by the rescalings below as $1/\vec{x}$.

Equations for $\lambda\phi^4$

For the model (3) we redefined the field and spacetime variables as

$$f_{pr} = \frac{a}{\phi_0}f, \quad \vec{x}_{pr} = \sqrt{\lambda}\phi_0\vec{x}, \quad dt_{pr} = \sqrt{\lambda}\phi_0\frac{dt}{a} \qquad (A10)$$

where $\phi_0 = 0.342 M_p$ is the value of the inflaton at the end of inflation (i.e., at the start of our simulations). This value was determined from linear numerical calculations as the point at which $\partial\phi_{pr}/\partial t_{pr} = 0$. For $\lambda = 9 \times 10^{-14}$ one unit of program (conformal) time is $a(\sqrt{\lambda}\phi_0)^{-1}t_{Planck} \sim a10^{-36}$ sec and one unit of program momentum is $a^{-1}\sqrt{\lambda}\phi_0 E_{Planck}$

$\sim a^{-1}10^{12}$ GeV, where a is the scale factor. In these variables the evolution equations became

$$\phi_{pr}'' - \nabla_{pr}^2 \phi_{pr} + \left(\phi_{pr}^2 + \frac{g^2}{\lambda}\chi_{i,pr}^2 - \frac{a''}{a} \right)\phi_{pr} = 0 \quad \text{(A11)}$$

$$\chi_{pr}'' - \nabla_{pr}^2 \chi_{pr} + \left(\frac{g^2}{\lambda}\phi_{pr}^2 + \frac{h_i^2}{\lambda}\sigma_{i,pr}^2 - \frac{a''}{a} \right)\chi_{pr} = 0 \tag{A12}$$

$$\sigma_{i,pr}'' - \nabla_{pr}^2 \sigma_{i,pr} + \left(\frac{h_i^2}{\lambda}\chi_{pr}^2 - \frac{a''}{a} \right)\sigma_{i,pr} = 0 \tag{A13}$$

$$a'' = -\frac{a'^2}{a} + \frac{8\pi\phi_0^2}{a}\left\langle \frac{1}{3}\sum_{fields}(|\nabla_{pr}f_{pr}|^2) + \frac{1}{4}\phi_{pr}^4 \right.$$
$$\left. + \frac{1}{2}\frac{g^2}{\lambda}\phi_{pr}^2\chi_{pr}^2 + \frac{1}{2}\frac{h_i^2}{\lambda}\chi_{pr}^2\sigma_{i,pr}^2 \right\rangle \tag{A14}$$

where primes denote differentiation with respect to t_{pr} and angular brackets denote spatial averages over the grid.

Equations for $m^2\phi^2$

For the model (23) we used the following redefinitions:

$$f_{pr} = \frac{a^{3/2}}{\phi_0}f, \quad \vec{x}_{pr} = m\vec{x}, \quad dt_{pr} = m\,dt \tag{A15}$$

where in this case $\phi_0 = 0.193M_p$. For $m = 10^{-6}M_p$ a unit of

program time corresponded to $m^{-1}T_{Planck} \sim 10^{-30}$ sec and a unit of program momentum corresponded to $a^{-1}mE_{Planck} \sim a^{-1}10^{13}$ GeV. The evolution equations became

$$\phi_{pr}'' - a^{-2}\nabla_{pr}^2\phi_{pr} - \frac{3}{4}\left(\frac{a'}{a}\right)^2\phi_{pr} - \frac{3}{2}\frac{a''}{a}\phi_{pr} + \phi_{pr}$$
$$+ \frac{g^2}{m^2}\phi_0^2 a^{-3}\chi_{pr}^2\phi_{pr} = 0 \tag{A16}$$

$$\chi_{pr}'' - a^{-2}\nabla_{pr}^2\chi_{pr} - \frac{3}{4}\left(\frac{a'}{a}\right)^2\chi_{pr} - \frac{3}{2}\frac{a''}{a}\chi_{pr} + \phi_0^2 a^{-3}$$
$$\times \left(\frac{g^2}{m^2}\phi_{pr}^2 + \frac{h_i^2}{m^2}\sigma_{i,pr}^2 \right)\chi_{pr}$$
$$= 0 \tag{A17}$$

$$\sigma_{i,pr}'' - a^{-2}\nabla_{pr}^2\sigma_{i,pr} - \frac{3}{4}\left(\frac{a'}{a}\right)^2\sigma_{i,pr} - \frac{3}{2}\frac{a''}{a}\sigma_{i,pr}$$
$$+ \frac{g^2}{m^2}\phi_0^2 a^{-3}\chi_{pr}^2\sigma_{i,pr} = 0 \tag{A18}$$

$$a'' = -2\frac{a'^2}{a} + \frac{8\pi\phi_0^2}{a^4}\left\langle \frac{1}{3}\sum_{fields}(|\nabla_{pr}f_{pr}|^2) + \frac{1}{2}a^2\phi_{pr}^2 \right.$$
$$\left. + \frac{1}{2}\phi_0^2 a^{-1}\left(\frac{g^2}{m^2}\phi_{pr}^2\chi_{pr}^2 + \frac{h_i^2}{m^2}\chi_{pr}^2\sigma_{i,pr}^2 \right) \right\rangle. \tag{A19}$$

[1] A. D. Linde, *Particle Physics and Inflationary Cosmology* (Harwood, Chur, Switzerland, 1990).

[2] A. Linde, Phys. Lett. B **259**, 38 (1991); Phys. Rev. D **49**, 748 (1994).

[3] L. Kofman, A. Linde, and A. Starobinsky, Phys. Rev. Lett. **73**, 3195 (1994).

[4] L. Kofman, A. Linde, and A. Starobinsky, Phys. Rev. D **56**, 3258 (1997).

[5] J. Garcia-Bellido, G. Felder, P. Greene, L. Kofman, A. Linde, and I. Tkachev (in preparation).

[6] S. Yu. Khlebnikov and I. Tkachev, Phys. Rev. Lett. **77**, 219 (1996).

[7] T. Prokopec and T. Roos, Phys. Rev. D **55**, 3768 (1997).

[8] T. Biró, S. Matinyan, and B. Müller, *Chaos and Gauge Field Theory* (World Scientific, Singapore, 1994).

[9] P. Greene, L. Kofman, A. Linde, and A. Starobinsky, Phys. Rev. D **56**, 6175 (1997).

[10] D. Boyanovsky, H. deVega, R. Holman, D. Lee, A. Singh, and J. Salgado, Phys. Rev. D **54**, 7570 (1996).

[11] G. Felder and I. Tkachev, Latticeasy software, 2000 (in preparation).

[12] V. Zakharov, V. L'vov, and G. Falkovich, *Wave Turbulence* (Springer-Verlag, Berlin, 1992).

[13] J. Garcia-Bellido, D. Grigoriev, A. Kusenko, and M. Shaposhnikov, Phys. Rev. D **60**, 123504 (1999).

[14] D. Polarski and A. Starobinsky, Class. Quantum Grav. **13**, 377 (1996).

[15] J. Garriga and A. Vilekin, Phys. Rev. D **56**, 2464 (1997).

[16] P. Greene and L. Kofman, Phys. Lett. B **448**, 6 (1999); Phys. Rev. D **62**, 123516 (2000).

[17] G. Aarts, G. Bonini, and C. Wetterich, Nucl. Phys. **B587**, 403 (2000).

[18] D. Semikoz and I. Tkachev, Phys. Rev. D **55**, 489 (1997).